Stochastic resonance for adhesion of membranes with active stickers

B. Różycki[1,2,a], T.R. Weikl[1], and R. Lipowsky[1]

[1] Max Planck Institute of Colloids and Interfaces, Science Park Golm, 14424 Potsdam, Germany
[2] Institute of Theoretical Physics, Warsaw University, Hoża 69, 00 681 Warszawa, Poland

Abstract. The behavior of two membranes that interact by active adhesion molecules or stickers is studied theoretically using mean-field theory and Monte Carlo simulations. The stickers are anchored in one of the membranes and undergo conformational transitions between on and off states. In their on states, the stickers can bind to ligands that are anchored in the other membrane. The transitions between the on and off states arise from the coupling of the stickers to some active, energy-releasing process, which keeps the system out of equilibrium. As one varies the transition rates of this active process, the membrane separation undergoes a stochastic resonance: this separation is maximal at intermediate rates of the sticker transitions and considerably smaller both at high and at low transition rates. This implies that the effective, fluctuation-induced repulsion between the membranes contains a rate-dependent contribution that arises from the switching of the active stickers.

PACS. 87.16.Dg Membranes, bilayers, and vesicles – 05.40.-a Fluctuation phenomena, random processes, noise, and Brownian motion – 87.68.+z Biomaterials and biological interfaces

1 Introduction

Biological membranes mainly consist of a fluid lipid bilayer which provides their basic structure and contains different macromolecules, mostly proteins [1,2]. Some of the proteins anchored in the lipid bilayer protrude from the membrane surface and can locally interact with another membrane, or a substrate surface. The influence of such adhesion or sticker molecules on membrane adhesion has been theoretically studied for some time [3–10]. The first kinetic model for the association and dissociation of membrane-anchored adhesion molecules was introduced in [3]. In the latter model, the only interactions between different adhesive bonds arise indirectly via an external force that pulls the membranes apart. In order to include the mutual interactions between different adhesion molecules anchored in the same membrane, we have introduced and studied lattice gas models for these systems [4–6]. Somewhat different theoretical approaches have been used in references [7,8], and force-induced membrane unbinding has been theoretically elucidated in references [9,10].

In all of these studies, the sticker molecules were assumed to have a single molecular conformation which is characterized by a certain binding energy. Biological membranes are, however, coupled to various processes such as

ATP hydrolysis which drive the membranes out of equilibrium. As a result, some adhesion molecules such as integrins can be switched between different conformational states with distinct affinities for their ligands [11–13].

In the following, we study such active stickers and their influence on membrane adhesion. In this context, the term "active" means that the transitions between different sticker states arise from their coupling to non-equilibrium processes. Other examples for active membrane components are provided by mobile ion channels [14,15], light-driven proton pumps [16] or two-state active inclusions which locally perturb the membrane curvature [17].

The adhesion or sticker molecules are anchored or embedded in one of the membranes and can bind to their ligands which are present in the other membrane, see Figure 1. Each sticker can attain two states: an "on" state in which the sticker interacts with its ligands in the opposite membrane, and an "off" state in which this interaction is negligible. Transitions between these states are not governed directly by thermal fluctuations but require energy input. In the case of active adhesion molecules in cell membranes, the energy input is usually provided by ATP hydrolysis that occurs in the cells, whereas in biomimetic applications, the conformational transitions of appropriately designed stickers may be triggered by light or external electric field [18–20]. These actively induced sticker transitions, in principle, can affect membrane adhesion in
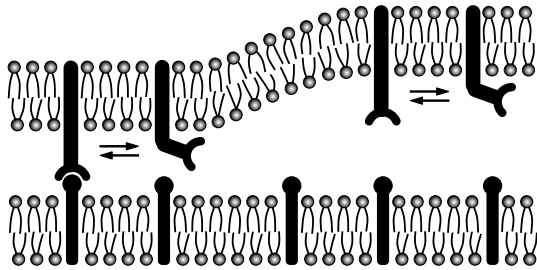
a e-mail: Bartosz.Rozycki@fuw.edu.pl

Fig. 1. A membrane with active stickers (top) adhering to another membrane (bottom). Each sticker can undergo transitions between two conformational states: an "on" state (stretched) in which the sticker can bind to ligands that are present in the other membrane, and an "off" state (bent) in which the interaction between the sticker and its ligands is negligible. These transitions require energy input and keep the system out of equilibrium.

a non-trivial way. The goal of this work is to study, both qualitatively and quantitatively, their influence on the average membrane separation.

In a recent letter [21] we studied the same system in the framework of a stochastic model with discrete time steps. The average membrane separation was found to exhibit a resonance when the typical time between sticker transitions was comparable to the relaxation time for short-wavelength membrane fluctuations. In the present paper, we consider a continuous-time Markov process as described by a Fokker-Planck equation and show that it exhibits a similar resonance as the discrete time model studied in reference [21]. Therefore, the resonance effect seems to be robust and essentially independent of the details of the model dynamics and, thus, should be a generic feature of the systems under consideration.

Another system with the same type of stochastic dynamics has also been recently used to study shape fluctuations of biomimetic membranes bound to a solid substrate by switchable crosslinker molecules [22]. In the latter case, the crosslinkers are switched between two conformations which have a different end-to-end distance. The statistical properties of the membrane separation are then governed by an effective potential with two competing minima. In contrast, the situation considered in the present study leads to an effective potential with a single, short-ranged potential well that is switched on and off.

This paper is organized as follows. In Section 2 we introduce a coarse-grained model for the aforementioned system, construct the Fokker-Planck equation that gives the model dynamics, and describe methods of computer simulations of this Fokker-Planck equation. In Section 3 we present results of our simulations and solve the Fokker-Planck equation numerically within the mean-field approximation. Both the results of our simulations and those obtained from the mean-field approximation indicate that the average membrane separation exhibits stochastic resonance: it is maximal at intermediate rates of the active process and considerably smaller at high or low transition rates. We investigate how the resonant behavior of the

system depends on the model parameters and summarize our results in Section 4.

2 Model

We consider a coarse-grained model that describes membranes as elastic sheets which form deformable but, on average, flat surfaces. To describe membrane configurations, a reference plane parallel to the two interacting membranes is introduced. Since we want, eventually, to study our model by computer simulations, the reference plane is divided into a square lattice with lattice constant a. Each lattice site is labeled by a pair of integer numbers $i = (x, y)$ with $1 \leq x \leq N$, $1 \leq y \leq N$ and periodic boundary conditions in both directions. The distance between the membranes at the lattice site i is denoted by $l_i > 0$. The set of variables $l = \{l_i\}$ thus specifies the relative membrane location. Then the elastic energy of the membranes can be written as [6]

$$\mathcal{H}_{\mathrm{el}}\{l\} = \sum_i \frac{\kappa}{2a^2}(\Delta_d l_i)^2, \tag{1}$$

where $\kappa = \kappa_1 \kappa_2/(\kappa_1 + \kappa_2)$ denotes the effective bending rigidity of the membranes with rigidities κ_1 and κ_2, while the discrete version of the Laplace operator,

$$\Delta_d l_{x,y} = l_{x+1,y} + l_{x-1,y} + l_{x,y+1} + l_{x,y-1} - 4l_{x,y}, \tag{2}$$

captures the local mean curvature of the separation field l.

In order to construct a model for the multi-state stickers that are present in one of the membranes, we introduce an additional set of discrete variables $n = \{n_i\}$, where n_i indicates the internal state of the sticker located over the lattice site i. For simplicity, we assume here that each lattice site is occupied by a sticker that has only two conformations. Then the lattice spacing a corresponds to the lateral distance between stickers and each of the variables n_i has only two possible values: 0 or 1. Here, $n_i = 0$ and $n_i = 1$ correspond to the "off" and "on" states, respectively, of the sticker at the lattice site i.

As described in the introduction, we consider the system where the stickers anchored in one of the membranes interact with the ligands on the other membrane. The short-range interaction between a sticker and a ligand depends on the relative position of the two molecules and on the sticker state. Thus, the energy of the overall interaction between the membranes at the lattice site i, which is denoted here by $V(l_i, n_i)$, depends on the local membrane separation l_i and on the internal state n_i of sticker at this site. The total energy of the system in a given configuration

$$\mathcal{H}\{l, n\} = \mathcal{H}_{\mathrm{el}}\{l\} + \sum_i V(l_i, n_i), \tag{3}$$

contains then —in addition to the bending energy— the term describing the intermembrane forces.

The sticker present at the lattice site i can bind to a ligand only when it is in the state "on" ($n_i = 1$). If the sticker at the lattice site i is in the state "off" ($n_i = 0$),
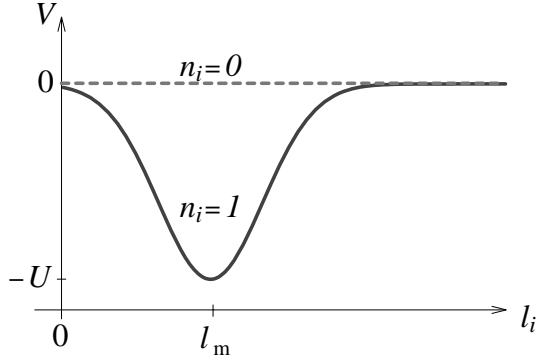
Fig. 2. Short-range sticker potential V as a function of the local membrane separation l_i. This potential has the Gaussian shape as given by (5) for $n_i = 1$ and vanishes for $n_i = 0$. A sticker in the state "on" ($n_i = 1$) thus attracts the membranes locally towards the potential minimum at $l_i = l_{\mathrm{m}}$, whereas a sticker in the state "off" does not mediate interactions between the membranes. Transitions between the sticker states correspond to switching the potential V_1 on and off.

the local interaction between the membranes at this site is negligible. Thus, we further assume that for $l_i > 0$ the sticker potential

$$V(l_i, n_i) = n_i V_1(l_i) \tag{4}$$

vanishes for $n_i = 0$ while for $n_i = 1$ it is given by the Gaussian function

$$V_1(l_i) = -U \exp\left[-\frac{(l_i - l_{\mathrm{m}})^2}{2l_{\mathrm{we}}^2}\right]. \tag{5}$$

The positive parameters l_{m}, l_{we} and U represent the potential range, width and depth, respectively. The profile of potential (4) is depicted in Figure 2.

2.1 Stochastic dynamics

2.1.1 Thermal motion

The two interacting membranes are embedded in an aqueous solution and are, thus, subject to thermal collisions with the water molecules. This leads to thermally excited deformations of the membrane shapes [23–25]. In the framework of the geometric membrane models considered here, these deformations are described by changes in the membrane separation field l. In general, there can be several mechanisms that contribute to the dissipation of the shape fluctuations of the membranes such as Stokes friction arising from the coupling to the surrounding liquid and interbilayer dissipation arising from the friction between the two adjacent monolayers [26,27]. We will consider the simplest type of dynamics which corresponds to the relaxation of the separation variables l_i along the gradients of the configuration energy $\mathcal{H}$ of the interacting membranes [28,6]. In the context of polymers and critical phenomena, this corresponds to Rouse dynamics [29] and

to the so-called model-A dynamics [30], respectively. The corresponding Langevin equation is given by

$$\phi\frac{\partial l_i}{\partial t} = -\frac{\partial \mathcal{H}}{\partial l_i} + \eta_i, \tag{6}$$

where ϕ is the viscous friction coefficient and η_i represents the white Gaussian noise. For the configuration energy $\mathcal{H}$ as given by (1–4), equation (6) takes the explicit form

$$\phi\frac{\partial l_i}{\partial t} = -\frac{\kappa}{a^2}\Delta_d^2 l_i - n_i\frac{\partial V_1}{\partial l_i} + \eta_i \tag{7}$$

and has a clear physical interpretation. It describes the overdamped motion of the separation variable l_i as a result of three types of forces: i) the elastic restoring force

$$-\frac{\partial \mathcal{H}_{\mathrm{el}}}{\partial l_i} = -\frac{\kappa}{a^2}\Delta_d^2 l_i \tag{8}$$

with

$$\begin{aligned}
\Delta_d^2 l_{x,y} = {}&(l_{x+2,y} + l_{x-2,y} + l_{x,y+2} + l_{x,y-2}) \\
&+ 2(l_{x+1,y+1} + l_{x-1,y+1} + l_{x+1,y-1} + l_{x-1,y-1}) \\
&- 8(l_{x+1,y} + l_{x-1,y} + l_{x,y+1} + l_{x,y-1}) + 20 l_{x,y}
\end{aligned} \tag{9}$$

which couples l_i with the separation variables at 12 neighboring lattice sites, ii) the force

$$-n_i\frac{\partial V_1}{\partial l_i}$$

which arises from the sticker potential $V_1(l_i)$ and vanishes when $n_i = 0$, and iii) the thermal white noise η_i. The average value of this latter noise vanishes at each lattice site, *i.e.*,

$$\langle\eta_i(t)\rangle = 0, \tag{10}$$

and its correlation function is given by

$$\langle\eta_i(t)\eta_{i'}(t')\rangle = 2\phi k_{\mathrm{B}}T\delta(t - t')\delta_{i,i'} \tag{11}$$

as required by the fluctuation-dissipation theorem (or the principle of detailed balance).

2.1.2 Active processes

So far, we have not specified how the stochastic variables $n_i(t)$ depend on time. In general, the stochastic field $n = \{n_i(t)\}$ could exhibit various spatial and temporal correlations. To ensure consistency with our recent membrane models [21,22], however, the active processes that occur in the system will be described here in the same way as in reference [22]. Below we repeat this description in order to make the present paper self-contained.

The variables $n_i(t)$ at different lattice sites are taken to be statistically independent of each other and to have temporal correlations that decay with a single characteristic time scale. More precisely, we will consider, at each lattice site i, the so-called dichotomic process (or two-valued Markov process or random telegraph process) [31].
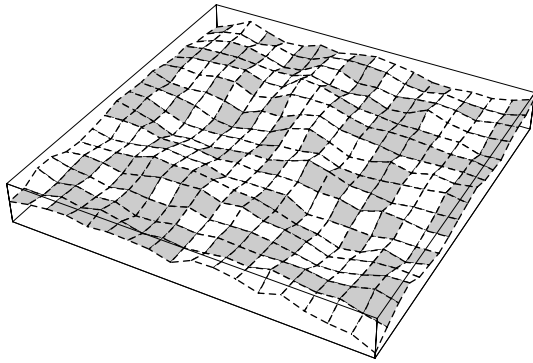
Fig. 3. Snapshot of one of the flexible membranes for a given state $\{n_i\}$ of the active stickers. At each lattice site i, a sticker molecule is present that can be in the state "on" ($n_i = 1$) or "off" ($n_i = 0$). The white and gray membrane patches correspond to $n_i = 0$ and $n_i = 1$, respectively. The time evolution of the sticker states is characterized by two transition rates as described in the main text.

For this process, the probabilities $p_1(t)$ and $p_0(t)$ to find the sticker at lattice site i at time t in the "on" and "off" state, respectively, satisfy the simple evolution equations

$$\frac{dp_1}{dt} = -p_1\,\omega_- + p_0\,\omega_+\,, \quad \frac{dp_0}{dt} = +p_1\,\omega_- - p_0\,\omega_+\,, \quad (12)$$

which depend on the two transition rates ω_+ and ω_-. The transition rate ω_+ represents the probability per unit time to go from the "off" state $n_i = 0$ to the "on" state $n_i = 1$. Likewise, the transition rate ω_- represents the probability per unit time for the reverse process from the "on" state $n_i = 1$ to the "off" state $n_i = 0$ (see Fig. 3). These transition rates are taken to be the same for all lattice sites i and for all values of the membrane displacement variables l_i. They characterize the energy-providing processes that are coupled to the switchable stickers, and depend on such quantities as concentration of ATP molecules in the membrane environment (in the case of active adhesion molecules present in the cell membranes) or light intensity (if the stickers are activated by photons).

In order to discuss the statistical properties of our model, it will be convenient to use the variable

$$X \equiv \frac{\omega_+}{\omega_+ + \omega_-}\,, \quad (13)$$

which describes the average fraction of "on" sites in the stationary state, and the mean transition rate

$$\omega \equiv \frac{\omega_+ + \omega_-}{2} \quad (14)$$

instead of the two transition rates ω_+ and ω_-. Here and below, X and ω will be considered as the basic transition parameters.

2.1.3 Thermal versus active fluctuations

If $\omega_- = 0$, the sticker transitions to the state "off" with $n_i = 0$ do not occur and, in the stationary case, all stickers

remain in their "on" state. Then $X = 1$ and the Langevin dynamics as given by (6) describes the relaxation of the membrane separation field in the laterally uniform potential $V_1(l_i)$. The membranes then attain a certain equilibrium state and relax to the potential well after a sufficiently long time. In such an equilibrium state, the separation variables l_i will undergo thermal fluctuations which are governed by the thermal energy k_BT.

In general, we will consider active processes which are characterized by an "on" fraction X with $0 < X < 1$ and a mean transition rate ω with $0 < \omega < \infty$. These processes induce additional membrane fluctuations which are not governed by the thermal energy k_BT but by the transition parameters X and ω. In other words, in the presence of the active, energy-consuming processes, configurational energy (3) is a functional of the time-dependent field $\{n_i(t)\}$. The membranes then are subject to time-dependent forces which drive the system out of equilibrium.

2.2 Fokker-Planck equation

The model dynamics as introduced in the previous subsection is given by

a) the Langevin-type equation (6) which describes the thermal motion of the membrane separation field l,
b) the definition of the stochastic variables n that describe random transitions between the sticker states.

The dynamics of our model can be also given by a corresponding Fokker-Planck equation [32]. The latter equation describes the evolution of the probability distribution $\mathcal{P}\{l,n,t\}$ for finding the system in the given configuration $\{l_i, n_i\}$ at time t. In order to construct the Fokker-Planck equation let us notice that the probability distribution $\mathcal{P}\{l,n,t\}$ changes in time

a) due to membrane diffusion and membrane drift along the gradients of the configuration energy $\mathcal{H}$,
b) as a result of the actively induced transitions between different sticker states.

The above statement can be written as a continuity equation for the probability distribution,

$$\frac{\partial \mathcal{P}}{\partial t} = \sum_i (I_i + \mathcal{I}_i). \quad (15)$$

The probability current density I_i, related to the i-th lattice site and corresponding to the Langevin dynamics (6), is obtained from the Smoluchowski or Fokker-Planck equation [32]

$$I_i\{l,n,t\} = \frac{1}{\phi}\frac{\partial}{\partial l_i}\left(\frac{\partial \mathcal{H}}{\partial l_i} + k_BT\frac{\partial}{\partial l_i}\right)\mathcal{P}\{l,n,t\}. \quad (16)$$

The first and second term on the right-hand side of equation (16) describe membrane drift along the gradients of $\mathcal{H}$ and membrane diffusion, respectively. The probability current density $\mathcal{I}_i$ is related to the active process at site i and can be determined from the master equation as described

below. Let us introduce an auxiliary set n' of two-valued variables n'_j, where the subscript j labels the lattice sites, such that $n'_j = n_j$ for all $j \neq i$ and $n'_i = 1 - n_i$. Then, as an obvious consequence of definition (12) of the two-valued Markov process, we have

$$\mathcal{I}_i\{l, n, t\} = \mathcal{I}_i^{\mathrm{off}}\{l, n, t\}\, \delta(n_i - 1) + \mathcal{I}_i^{\mathrm{on}}\{l, n, t\}\, \delta(n_i) \quad (17)$$

with

$$\mathcal{I}_i^{\mathrm{off}}\{l, n, t\} \equiv \mathcal{P}\{l, n'(n), t\}\, \omega_+ - \mathcal{P}\{l, n, t\}\, \omega_- \quad (18)$$

and

$$\mathcal{I}_i^{\mathrm{on}}\{l, n, t\} \equiv \mathcal{P}\{l, n'(n), t\}\, \omega_- - \mathcal{P}\{l, n, t\}\, \omega_+. \quad (19)$$

At this point one should also notice that the variables n_i and l_i that appear in equations (15–19) are no longer functions of time; both n and l are treated here as independent coordinates for the probability distribution $\mathcal{P}$.

In the stationary case, equations (15–19) supplemented by the proper boundary conditions can be solved numerically in the framework of mean-field approximation. This stationary solution is presented in Section 3.2. The model dynamics expressed by the Fokker-Planck equation is also used to establish the procedure of Monte Carlo simulations of our model. We present the latter approach in the following subsection.

2.3 Monte Carlo simulation and master equation

The statistical properties of the membrane model introduced in this section can be studied by Monte Carlo simulations [33]. It is then useful to define the dimensionless separation variable [28]

$$z_i \equiv \frac{l_i}{a}\sqrt{\frac{\kappa}{k_\mathrm{B}T}} \quad (20)$$

at each lattice site i and to rewrite the configuration energy (3) in terms of these variables. The membrane shape is now specified by the set $z = \{z_i\}$.

As before, we consider a discrete lattice of $N \times N$ sites. Each lattice site is labeled by a pair of integer numbers $i = (x, y)$ with $1 \leq x \leq N$, $1 \leq y \leq N$ and periodic boundary conditions in both the x and the y directions. The Monte Carlo (MC) simulations described here have been performed with up to 10^8 MC steps, *i.e.*, MC moves per lattice site.

Each MC move consists of two submoves: i) First, a lattice site, i, is randomly chosen, and the membrane separation at this site, z_i, is shifted to the value $z_i + \zeta$, where ζ is a random number with the probability distribution $p(\zeta) = 1/(2\,\delta z)$ for $-\delta z < \zeta < \delta z$, and δz is the step size for the separation variable. This submove is accepted according to the standard Metropolis algorithm [33] with probability

$$w\{z \to z'\} = \min\left[1, \exp\left(-\frac{\mathcal{H}\{z', n\} - \mathcal{H}\{z, n\}}{k_\mathrm{B}T}\right)\right], \quad (21)$$

where the new, primed separation variables are defined by $z'_j \equiv z_j + \delta_{i,j}\,\zeta$. The submoves for which $z_i + \zeta < 0$ are rejected. In this way we capture in our simulations the reflecting boundary conditions at $z_i = 0$. ii) The second submove consists of the random choice of another lattice site j for which the value of the variable n_j is switched from $n_j = 1$ to $n_j = 0$ with probability Ω_- and vice versa with probability Ω_+.

It has been previously argued that the Metropolis algorithm has the same scaling properties as the Langevin dynamics [28] since both describe the relaxational dynamics along the gradients of the configuration energy. However, we will now show that it is even possible to derive a quantitative mapping between the Metropolis algorithm just described and the Langevin dynamics as given by (6). This mapping is obtained in the limit of small δz, *i.e.*, of small step size for the separation variables z_i, and leads to explicit relations between the simulation parameters $\delta z, \Omega_+, \Omega_-$ and the parameters ϕ, ω_+, ω_-, which appear in the continuous-time model.

In order to derive this mapping, let us consider the probability distribution $\mathcal{P}\{z, n, t\}$ for the membrane configuration $\{z_i, n_i\}$ at time t. The probability current density $I_i\{z, n, t\}$, which is induced by the first submove i) as described above, satisfies the master equation

$$I_i\{z, n, t\}\delta t = \frac{1}{2\,\delta z}\int_{-\delta z}^{\delta z}\mathrm{d}\zeta\left[\mathcal{P}\{z', \mathrm{n}, \mathrm{t}\}\,\mathrm{w}\{z' \to z\}\right.$$
$$\left. -\mathcal{P}\{z, n, t\}w\{z \to z'\}\right] \quad (22)$$

with the time step δt corresponding to one submove and the transition probabilities $w\{z' \to z\}$ as in (21). The first and second terms in the square brackets describe the gain and loss of the probability density, respectively. In order to make a connection with the continuous-time model corresponding to the Langevin dynamics (6), we will now consider the limit of small time step δt and small step size δz for the displacement variables.

We thus expand the probability distribution $\mathcal{P}$ and the transition probabilities w, which are present on the right-hand side of equation (22), in powers of the dimensionless variable ζ which is then integrated between $-\delta z$ and $+\delta z$. This calculation is presented in the appendix and leads to the truncated master equation

$$I_i\{z, n, t\}\delta t = \frac{(\delta z)^2}{6}\frac{\partial}{\partial z_i}\left(\frac{1}{k_\mathrm{B}T}\frac{\partial\mathcal{H}}{\partial z_i} + \frac{\partial}{\partial z_i}\right)\mathcal{P}\{z, n, t\}$$
$$+ O((\delta z)^3). \quad (23)$$

On the other hand, the probability current density which corresponds to the Langevin dynamics for the membrane separation l_i as given by (6) has the Smoluchowski or Fokker-Planck form (16). Comparing expression (23) with (16) and using equation (20), we obtain the parameter relation

$$\delta t = \frac{(\delta z)^2}{6}\frac{\phi a^2}{\kappa}. \quad (24)$$

If this relation is fulfilled, the Langevin dynamics as given by (6) and the Metropolis dynamics as in (21) are equivalent in the limit of small step size $\delta z \sim (\delta t)^{1/2}$.

Since we alternate between submove i) and submove ii), the same time step δt is used for both submoves. This implies that the switching probabilities $\Omega_\pm$ and the transition rates $\omega_\pm$ are related via

$$\Omega_\pm = \delta t\, \omega_\pm = \frac{(\delta z)^2}{6} \frac{\phi a^2}{\kappa} \omega_\pm. \qquad (25)$$

In the long-time limit the system attains a steady state which is characterized by certain time-independent quantities such as the average membrane separation $\langle z \rangle$ and the two-point correlation function $\langle z_i z_j \rangle - \langle z_i \rangle \langle z_j \rangle$. We determine these steady-state quantities from the Monte Carlo simulations. In a recent work [22] we used the same simulation procedure and showed that for a harmonic potential $V(z_i, n_i)$ the simulation results agree with an analytical solution.

For all Monte Carlo simulations reported below, the step size δz was chosen to be $\delta z = 2.5 \times 10^{-3}$. In addition, we used the system size $N = 40$ and checked that this size is sufficiently large so that our data are not affected by finite-size effects.

3 Results

3.1 Simulation results

To describe the simulation results, let us first consider what could be the influence of the active process on the membrane separation. In the hypothetical situation when the thermal fluctuations are absent, $T = 0$, the membranes would drift from their initial configurations towards the minimum of potential (5) and remain at $l_i = l_m$. Thermal fluctuations cause, however, accidental collisions between the membranes. These collisions lead to an effective steric repulsion between the membranes. We can thus deduce that $\langle l \rangle > l_m$ for any $T > 0$. Moreover, if the temperature is increased, the membrane collisions become more violent, the steric repulsion gets then stronger and, consequently, the average membrane separation $\langle l \rangle$ increases as well. On the other hand, $\langle l \rangle$ decreases if attractive interactions between the membranes are made stronger. This can be achieved by increasing values of such parameters like the concentration X of stickers in the "on" state or the sticker binding energy U.

Consider now the case when only the transition rates ω_+ and ω_- may vary while values of other model parameters remain constant. One might expect that the membrane separation depends then only on the average fraction of stickers in their "on" state, $X = \omega_+/(\omega_+ + \omega_-)$. Our simulation results show, however, that even for a constant fraction X of "on" stickers, the average membrane separation $\langle l \rangle$ in the steady state changes with the mean transition rate ω. Examples of our simulation data are shown in Figure 4.
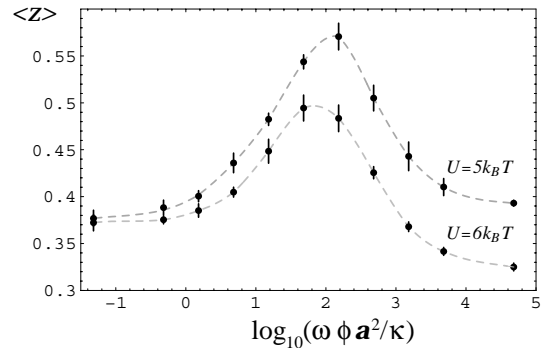

Fig. 4. Average membrane separation $\langle z \rangle$ in the steady state as a function of the average transition rate ω which is rescaled with the friction coefficient ϕ, the molecular size a, and the bending rigidity κ (semi-logarithmic plot). The average fraction of stickers in their "on" states is $X = 0.3$. The range and width of the sticker potential V_1 given by (5) are $z_m = 0.2$ and $z_{we} = 0.05$, respectively. The sticker binding energy is $U = 5k_BT$ (upper curve) and $U = 6k_BT$ (bottom curve). The dashed lines are plotted to guide the eye.
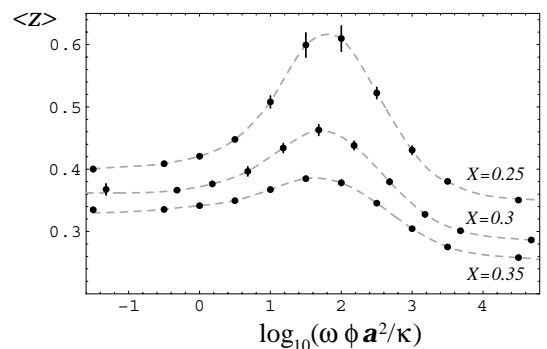

Fig. 5. Average membrane separation $\langle z \rangle$ in the steady state as a function of the average transition rate ω which is rescaled with the friction coefficient ϕ, the lattice constant a and the bending rigidity κ (semi-logarithmic plot). The range, width and depth of the sticker potential (5) are $z_m = 0.2$, $z_{we} = 0.05$ and $U = 7k_BT$, respectively. The average fraction of stickers in their "on" states is $X = 0.25$ (upper curve), $X = 0.3$ (middle curve) and $X = 0.35$ (bottom curve). The dashed lines are plotted to guide the eye. The resonance effect is strongly pronounced for small concentrations X.

It might seem astonishing that the membrane separation is maximal at intermediate values of ω. This effect has already been observed in our previous model [21] and turns out to be closely related to the process of resonant activation over a fluctuating energy barrier in one-particle models [34,35]. The typical time for a membrane patch to diffuse out of the potential range can be made minimal by a proper tuning of the transition rates. This implies that there exists an optimal value for the mean transition rate ω for which the membranes are most weakly bound. This fact is clearly reflected in Figure 4.

Our simulation data indicates also that the resonance is more prominent when the average fraction X of stickers in the "on" state is small (see Fig. 5). This effect is

understandable. A general feature of systems in the vicinity of a continuous phase transition is that small variations in control parameters lead to large changes of macroscopic quantities characterizing the systems. In our model, the membranes are weakly bound when the concentration X of "on" stickers is small. In this case, small variations of other model parameters, such as the potential depth U or the transition rate ω, lead to large changes in the average membrane separation.

3.2 Mean-field approximation for the Fokker-Planck equation

We shall now return to the formulation of the model dynamics given by the Fokker-Planck equation (15) and the definitions of the probability current densities (16–19). Our goal is now to solve these equations numerically within the framework of the mean-field theory proposed by Van den Broeck [36,37].

Let us consider the one-site stationary probability distribution, $P_\alpha(l_i)$ with $\alpha \in \{0,1\}$, for finding the membranes at distance l_i and the sticker in the state $n_i = \alpha$ at the lattice site i. Then $P(l_i) = P_0(l_i) + P_1(l_i)$ is the stationary probability distribution for finding the membranes at distance l_i over the lattice site i. The one-site probabilities can be obtained from the stationary probability distribution $\mathcal{P}\{l, n\}$ as follows:

$$P_\alpha(l_i) = \sum_{\{n_j\}}{}' \prod_{j \neq i} \int_0^\infty dl_j \mathcal{P}\{l, n\}, \qquad (26)$$

where the sign $\sum'_{\{n_j\}}$ denotes the sum over all possible values of variables $n = \{n_j\}$ with the condition $n_i = \alpha$.

Now, we integrate equation (15) over all variables $\{l_j\}$ except for l_i and then sum it over all variables $\{n_j\}$ except for n_i. Using next definitions (16–19) of the probability current densities I_i and $\mathcal{I}_i$, equations (1–4) for the configuration energy $\mathcal{H}$, and the reflecting boundary conditions at $l_i = 0$, leads to the following exact steady-state equations for the one-site probabilities:

$$\frac{\partial J_0}{\partial l_i} + P_0(l_i) \omega_+ - P_1(l_i) \omega_- = 0, \qquad (27)$$

$$\frac{\partial J_1}{\partial l_i} + P_1(l_i) \omega_- - P_0(l_i) \omega_+ = 0, \qquad (28)$$

where the probability currents J_0 and J_1 are defined as follows:

$$J_0(l_i) = -\frac{1}{\phi} \frac{\partial W}{\partial l_i} P_0(l_i) - \frac{k_B T}{\phi} \frac{\partial P_0}{\partial l_i}, \qquad (29)$$

$$J_1(l_i) = -\frac{1}{\phi} \left(\frac{\partial W}{\partial l_i} + \frac{\partial V_1}{\partial l_i} \right) P_1(l_i) - \frac{k_B T}{\phi} \frac{\partial P_1}{\partial l_i}. \qquad (30)$$

The energy $W(l_i)$ describes coupling of the sticker at site i with the membrane. Its derivative is given by

$$\frac{\partial W}{\partial l_i} = \prod_{j \neq i} \int_0^\infty dl_j \left[\frac{\partial \mathcal{H}_{el}}{\partial l_i} \mathcal{P}\{l|l_i\} \right], \qquad (31)$$

where the membrane bending energy $\mathcal{H}_{el}$ is given by equation (1) and $\mathcal{P}\{l|l_i\} = \mathcal{P}\{l\}/P(l_i)$ denotes the conditional probability distribution for the given configuration $l = \{l_j\}$ with the fixed variable l_i.

The above equations should be supplemented by the reflecting boundary conditions at $l_i = 0$, *i.e.*, at the membrane contact points,

$$J_0(0) = 0 \quad \text{and} \quad J_1(0) = 0. \qquad (32)$$

These conditions ensure that the membranes cannot penetrate each other. The additional set of boundary conditions,

$$\lim_{l_i \to \infty} J_0(l_i) = 0 \quad \text{and} \quad \lim_{l_i \to \infty} J_1(l_i) = 0, \qquad (33)$$

can be obtained by integrating (27) and (28) over dl_i in the limits from zero to infinity and using the normalization conditions of the one-site probability distributions:

$$\int_0^\infty P_0(l_i) dl_i = 1 - X \quad \text{and} \quad \int_0^\infty P_1(l_i) dl_i = X. \qquad (34)$$

The boundary conditions (32, 33) have been already used to derive equations (27–31) from the Fokker-Planck equation (15–19). These are the conditions (32, 33) that allow us to neglect the boundary terms after integration of (15) over all variables l except for l_i.

Note that equations (27) and (28) imply that the probability current $J = J_0(l_i) + J_1(l_i)$ is constant. Next, the boundary conditions (32) imply additionally that $J = 0$. Thus, in the stationary state, the relative average velocity of membranes vanishes.

So far we have not applied any approximation and the equations presented above are exact. However, the energy $W(l_i)$ as given by equation (31) depends on the conditional probability distribution $\mathcal{P}\{l|l_i\} = \mathcal{P}\{l\}/P(l_i)$ and, for this reason, we are not able to solve the set of equations (27–33). We therefore apply a simple approximation [37] which is analogous to the traditional mean-field theory. In this approximation, one neglects correlations between neighboring lattice sites so that

$$\mathcal{P}\{l|l_i\} = \prod_{j \neq i} P(l_j) \qquad (35)$$

which leads to a significant simplification of equation (31),

$$\frac{\partial W}{\partial l_i} = 20 \frac{\kappa}{a^2} (l_i - \langle l \rangle). \qquad (36)$$

The numerical factor 20 is a consequence of equation (9) for the spatial fourth derivative on the square lattice. In the framework of mean-field approximation (36), equations (27–30) supplemented by the boundary conditions (32, 33) and definition (5) of the sticker potential V_1 constitute a self-consistent set of equations for the average membrane separation

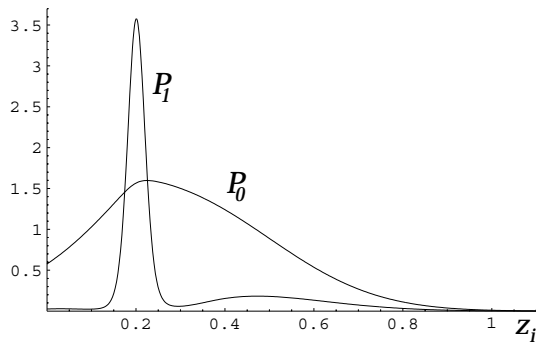$$\langle l \rangle = \int_0^\infty l_i \left[P_0(l_i) + P_1(l_i) \right] dl_i. \qquad (37)$$

Fig. 6. Probability distributions P_0 and P_1 for the dimensionless membrane separation z_i and the sticker state $n_i = 0$ and $n_i = 1$, respectively. The distributions have been determined in the framework on the mean-field approximation and represent a numerical solution of the self-consistent set of equations introduced in this section. The potential range, width and depth are $z_m = 0.2$, $z_{we} = 0.05$ and $U = 7k_BT$, respectively. The average fraction of "on" stickers is $X = 0.25$. The average transition rate is given by $\omega \phi a^2/\kappa = 25$, where ϕ is the friction coefficient, a is the lattice constant and κ is the effective bending rigidity. The transition rate as given by $\omega \phi a^2/\kappa = 25$ is approximately equal to the resonant frequency for the middle curve in Figure 8. The average membrane separation as given by (37) and obtained from the numerical integration with the distributions $P_0(z_i)$ and $P_1(z_i)$ is $\langle z \rangle \approx 0.31673$.
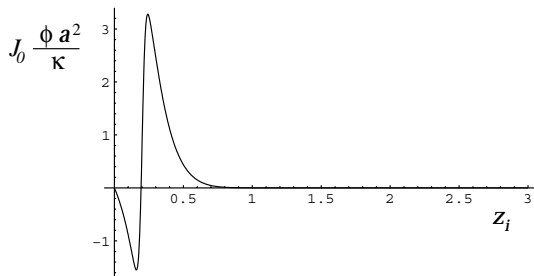

Fig. 7. The probability current J_0 rescaled with the friction coefficient ϕ, the lattice constant a and the bending rigidity κ as a function of the dimensionless membrane separation z_i. The probability current J_0 as plotted here is related via equation (29) to the probability distribution P_0 which is presented in Figure 6. The following boundary conditions are fulfilled: $J_0(0) = 0$ and J_0 vanishes for $z_i \gg z_m$. The numerical solution of the mean-field equations ensures that $J_0 + J_1 = 0$.

It is generally known that, for 2-dimensional membranes as considered here, the mean-field theory provides a reliable approximation as long as the membrane potential has a sufficiently deep potential well and the effective repulsion between the membranes arising from their shape fluctuations is sufficiently weak. Thus, we shall restrict our further considerations to the regimes in the model parameter space where the average membrane separation $\langle l \rangle$ is comparable with the distance l_m that describes the range of the sticker potential V_1 as given by equation (5). In this case it seems reasonable to replace boundary conditions (33) by the requirement that the probability currents $J_0(l_i)$ and $J_1(l_i)$ vanish for $l_i \gg l_m$. The mean-field equa-
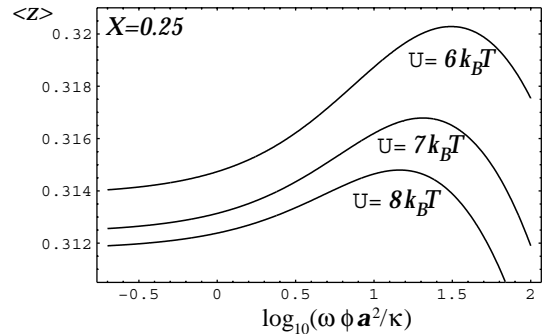

Fig. 8. Average membrane separation $\langle z \rangle$ in the stationary state as a function of the mean transition rate ω which is rescaled with the friction coefficient ϕ, lattice constant a and the effective bending rigidity κ. This plot represents numerical solutions of the Fokker-Planck equation in the mean-field approximation. The average fraction of stickers in their "on" state is $X = 0.25$. The potential range and width are $z_m = 0.2$ and $z_{we} = 0.05$, respectively. Depth of potential V_1 is $U = 6k_BT$ (upper curve), $U = 7k_BT$ (middle curve) and $U = 8k_BT$ (bottom curve). The resonance effect is relatively weak and suppressed by the mean-field approximation.
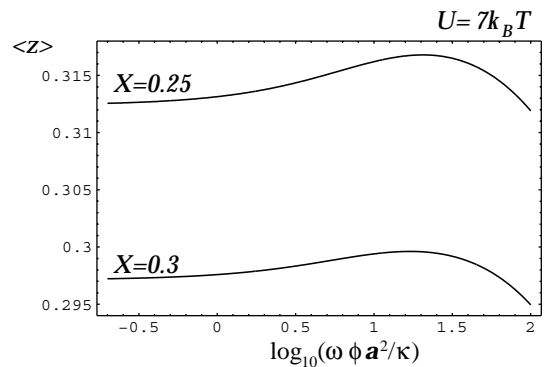

Fig. 9. Average membrane separation $\langle z \rangle$ in the stationary state as a function of the mean transition rate ω which is rescaled with the friction coefficient ϕ, lattice constant a and the effective bending rigidity κ. This plot represents numerical solutions of the Fokker-Planck equation in the mean-field approximation. The potential range, width and depth are $z_m = 0.2$, $z_{we} = 0.05$ and $U = 7k_BT$, respectively. The average fraction of stickers in their "on" state is $X = 0.25$ (upper curve) and $X = 0.3$ (bottom curve). The simulation results for the same model parameters are shown in Figure 5. Compared to these simulations, the mean-field approximation leads to a less pronounced resonance effect.

tions with such modified boundary conditions have been solved numerically by using *Mathematica*. Examples of the numerical results are depicted in Figures 6–9.

In Figure 6 we show the stationary probability distributions $P_0(z_i)$ and $P_1(z_i)$ for dimensionless membrane separation z_i and the sticker state $n_i = 0$ and $n_i = 1$, respectively. In Figure 7 we present the probability current J_0 that is related via equation (29) to the probability distribution P_0 which is presented in Figure 6. Here, the probability current J_0 is shown as a function of dimensionless membrane separation z_i. These two plots represent a

numerical solution of the mean-field equations for a given set of model parameters, as explained in the figure captions.

In Figures 8 and 9 the average membrane separation $\langle z \rangle$, given in dimensionless units, is shown as a function of the mean transition rate ω for several values of the sticker binding energy U and fraction X of stickers in the state "on".

The average membrane separation as presented in Figures 8 and 9 exhibits stochastic resonance. The mean-field predictions thus confirm the results of our MC simulations. However, comparison of Figures 5 and 9 shows that, compared to the MC simulations, the mean-field approximation gives smaller values for the average membrane separation. The mean-field theory thus underestimates the effective membrane repulsion which arises from the shape fluctuations of the membranes. This fluctuation-induced repulsion varies with the average transition rate ω, see Figures 5 and 9, and, thus, contains an ω-dependent contribution that arises from the switching of the active stickers.

4 Summary

We have presented a stochastic model for two membranes that interact by active adhesion molecules, or stickers. The stickers are anchored or embedded in one of the membranes and can bind to their ligands which are present in the other membrane. Each sticker can undergo actively induced transitions between two states: an "on" state in which the sticker interacts with the apposing membrane, and an "off" state in which this interaction is negligible. These transitions arise from the coupling of the stickers to some active, energy-releasing process, which keeps the system out of equilibrium.

Both the actively induced transitions between sticker states and the thermal motion of the membranes represent stochastic processes. We use the Langevin-type equation (6) in order to describe the overdamped motion of the membrane separation field, and the two-valued Markov process (12) in order to model the random transitions between different states of the stickers.

We have used both Monte Carlo simulations and mean-field theory to study the statistical properties of this model. Our results show that the actively induced sticker transitions affect the average membrane separation $\langle l \rangle$ in a non-trivial way: $\langle l \rangle$ is maximal at intermediate transition rates and considerably smaller at high or low rates of the active process.

In a recent letter [21], we studied a similar system in the framework of a stochastic model with discrete time steps. The average membrane separation was found to exhibit a similar resonance when the typical time between sticker transitions was comparable to the relaxation time for short-wavelength membrane fluctuations. Therefore, the resonance effect seems to be robust and insensitive to details of model dynamics and, thus, should be a generic feature of the systems under study.

B Equation (23)

Here we prove that for sufficiently small simulation step size, δz, equation (22) reduces to (23). As described in Subsection 2.3, the energy difference related to a MC move is

$$\delta \mathcal{H} = \mathcal{H}(z', n) - \mathcal{H}(z, n), \qquad (B.1)$$

where $z'_j = z_j + \zeta \delta_{i,j}$ and $\zeta \in [-\delta z, \delta z]$ is a small, dimensionless parameter. The potential V_1 as given by (5) is a smooth function of the membrane separation. This implies that $\delta \mathcal{H}$ is a smooth function and of parameter ζ and hence

$$\delta \mathcal{H} = \zeta \frac{\partial \mathcal{H}}{\partial z_i} + \frac{\zeta^2}{2} \frac{\partial^2 \mathcal{H}}{\partial z_i^2} + O(\zeta^3). \qquad (B.2)$$

The above derivatives with respect to the spatial variable z_i are taken at $\zeta = 0$.

To simplify the notation, let $D = [-\delta z, \delta z]$. Let us also introduce the set $D_< \subset D$, such that $\delta \mathcal{H} \leq 0$ for $\zeta \in D_<$. Then, according to definition (21) for the transition probability w, for $\zeta \in D_<$ we have $w(z' \to z) = \exp(\delta \mathcal{H}/k_B T)$ and $w(z \to z') = 1$. Similarly, let $D_> \subset D$ be such a set that $\delta \mathcal{H} > 0$ for $\zeta \in D_>$. In this case $w(z' \to z) = 1$ and $w(z \to z') = \exp(-\delta \mathcal{H}/k_B T)$. Since $D = D_< \cup D_>$ and $D_< \cap D_> = \emptyset$, equation (22) can be now written as follows:

$$I_i(z, n, t)\delta t = \frac{1}{2\delta z} \int_{D_<} \left[\mathcal{P}(z', n, t)e^{\delta \mathcal{H}/k_B T} - \mathcal{P}(z, n, t) \right] \mathrm{d}\zeta$$

$$+ \frac{1}{2\delta z} \int_{D_>} \left[\mathcal{P}(z', n, t) - \mathcal{P}(z, n, t)e^{-\delta \mathcal{H}/k_B T} \right] \mathrm{d}\zeta. \quad (B.3)$$

Expansion of the integrand up to second order in ζ leads to

$$I_i(z, n, t)\delta t = \frac{1}{2\delta z} \left[\left(\frac{\mathcal{P}}{k_B T} \frac{\partial^2 \mathcal{H}}{\partial z_i^2} + \frac{\partial^2 \mathcal{P}}{\partial z_i^2} \right) \int_D \frac{\zeta^2}{2} \mathrm{d}\zeta \right.$$

$$+ \frac{\mathcal{P}}{(k_B T)^2} \left(\frac{\partial \mathcal{H}}{\partial z_i} \right)^2 \left(\int_{D_<} \frac{\zeta^2}{2} \mathrm{d}\zeta - \int_{D_>} \frac{\zeta^2}{2} \mathrm{d}\zeta \right)$$

$$\left. + \frac{1}{k_B T} \frac{\partial \mathcal{P}}{\partial z_i} \frac{\partial \mathcal{H}}{\partial z_i} \int_{D_<} \zeta^2 \mathrm{d}\zeta + O((\delta z)^4) \right], \quad (B.4)$$

where we have used $\int_D \zeta \mathrm{d}\zeta = 0$. The above derivatives with respect to z_i are taken at $\zeta = 0$.

If $\frac{\partial \mathcal{H}}{\partial z_i} = 0$, then equation (B.4) simplifies to

$$I_i(z, n, t)\delta t = \frac{(\delta z)^2}{6} \left(\frac{\mathcal{P}}{k_B T} \frac{\partial^2 \mathcal{H}}{\partial z_i^2} + \frac{\partial^2 \mathcal{P}}{\partial z_i^2} \right) + O((\delta z)^3).$$
$$(B.5)$$

If $\frac{\partial \mathcal{H}}{\partial z_i} \neq 0$, then according to expansion (B.2), $\delta \mathcal{H} = 0$ when $\zeta = 0$ or $\zeta = -2\frac{\partial \mathcal{H}}{\partial z_i}/\frac{\partial^2 \mathcal{H}}{\partial z_i^2}$. Within the framework of approximation (B.2), the energy change $\delta \mathcal{H}$ plotted as a

function of the parameter ζ is a parabola and since $|\zeta| \leq \delta z$, we have for

$$\delta z < 2 \left| \frac{\frac{\partial \mathcal{H}}{\partial z_i}}{\frac{\partial^2 \mathcal{H}}{\partial z_i^2}} \right| \tag{B.6}$$

only two alternative cases:

1) $D_< = [0, \delta z]$ and $D_> = [-\delta z, 0]$,

2) $D_< = [-\delta z, 0]$ and $D_> = [0, \delta z]$.

In both cases equation (B.4) reduces to

$$I_i(z, n, t)\delta t = \frac{(\delta z)^2}{6} \left[\frac{\mathcal{P}}{k_{\mathrm{B}}T} \frac{\partial^2 \mathcal{H}}{\partial z_i^2} + \frac{\partial^2 \mathcal{P}}{\partial z_i^2} + \frac{1}{k_{\mathrm{B}}T} \frac{\partial \mathcal{H}}{\partial z_i} \frac{\partial \mathcal{P}}{\partial z_i} \right]$$
$$+ O((\delta z)^3). \tag{B.7}$$

Both equations (B.5) and (B.7) can be rewritten as (23). Thus, for sufficiently small simulation step size δz, when inequality (B.6) is fulfilled, equation (22) reduces to (23), *quod erat demonstrandum.*

References

1. B. Alberts, A. Johnson, J. Lewis, M. Raff, K. Roberts, P. Walter, *Molecular Biology of the Cell*, fourth edition (Garland Science, New York, 2002)
2. R. Lipowsky, E. Sackmann (Editors), *Structure and Dynamics of Membranes* (Elsevier, Amsterdam, 1995)
3. G.I. Bell, Science **200**, 618 (1978)
4. R. Lipowsky, Phys. Rev. Lett. **77**, 1652 (1996)
5. T.R. Weikl, R.R. Netz, R. Lipowsky, Phys. Rev. E **62**, R45 (2000)
6. T.R. Weikl, R. Lipowsky, Phys. Rev. E **64**, 011903 (2001)
7. S. Komura, D. Andelman, Europhys. Lett. **64**, 844 (2003)
8. H.-Y. Chen, Phys. Rev. E **67**, 031919 (2003)
9. U. Seifert, Phys. Rev. Lett. **82**, 2750 (2000)
10. T. Erdmann, U.S. Schwarz, Phys. Rev. Lett. **92**, 108102 (2004)
11. M.L. Dustin, T.G. Bivona, M.R. Philips, Nat. Immunology **5**, 363 (2004)
12. J. Takagi, B.M. Petre, T. Walz, T.A. Springer, Cell **110**, 599 (2002)
13. M. Kim, C.V. Carman, T.A. Springer, Science **301**, 1720 (2003)
14. J. Prost, R. Bruinsma, Europhys. Lett. **33**, 321 (1996)
15. J. Prost, J.-B. Manneville, R. Bruinsma, Eur. Phys. J. B **1**, 465 (1998)
16. N. Gov, S. Safran, Phys. Rev. E **69**, 011101 (2004)
17. H.-Y. Chen, Phys. Rev. Lett. **92**, 168101 (2004)
18. G. Möller, M. Harke, H. Motschmann, Langmuir **14**, 4955 (1998)
19. K. Ichimura, S.-K. Oh, M. Nakagawa, Science **288**, 1624 (2000)
20. S. Abbott, J. Ralston, G. Reynolds, R. Hayes, Langmuir **15**, 8923 (1999)
21. B. Różycki, R. Lipowsky, T.R. Weikl, Phys. Rev. Lett. **96**, 048101 (2006)
22. B. Różycki, T.R. Weikl, R. Lipowsky, Phys. Rev. E **73**, 061908 (2006)
23. J. Rädler, T.J. Feder, H.H. Strey, E. Sackmann, Phys. Rev. E. **51**, 4526 (1995)
24. B. Pozo-Navas, V.A. Raghunathan, J. Katsaras, M. Rappolt, K. Lohner, G. Pabst, Phys. Rev. Lett. **91**, 028101 (2003)
25. H.-G. Döbereiner, G. Gompper, C.K. Haluska, D.M. Kroll, P.G. Petrov, K. Riske, Phys. Rev. Lett. **91**, 48301 (2003)
26. U. Seifert, S.A. Langer, Europhys. Lett. **23**, 71 (1993)
27. U. Seifert, S.A. Langer, Biophys. Chem. **49**, 13 (1994)
28. R. Lipowsky, B. Zielinska, Phys. Rev. Lett. **62**, 1572 (1989)
29. M. Doi, S.F. Edwards, *The Theory of Polymer Dynamics*, (Clarendon Press, Oxford, 1986)
30. P.C. Hohenberg, B.I. Halperin, Rev. Mod. Phys. **49**, 435 (1977)
31. N. van Kampen, *Stochastic Processes in Physics and Chemistry* (Elsevier, Amsterdam, 1992)
32. H. Risken, *The Fokker-Planck Equation: Methods of Solution and Applications* (Springer-Verlag, Berlin, 1989)
33. K. Binder, D.W. Heermann, *Monte Carlo Simulation in Statistical Physics* (Springer-Verlag, Berlin, 1992)
34. Ch.R. Doering, J.C. Gadoua, Phys. Rev. Lett. **69**, 2318 (1992)
35. A. Mielke, Phys. Rev. Lett. **84**, 818 (2000)
36. C. Van den Broek, J.M.R. Parrondo, R. Toral, Phys. Rev. Lett. **73**, 3395 (1994)
37. C. Van den Broek, J.M.R. Parrondo, R. Toral, R. Kawai, Phys. Rev. E. **55**, 4084 (1997)